Mathematical model for rod outer segment dynamics during retinal detachment and reattachment

William Ebo Annan[1☯], Emmanuel O.A. Asamani [1☯], Diana White [1☯*],

1 Department of Mathematics, Clarkson University, 8 Clarkson Avenue, Potsdam, NY, 13699, USA.

☯These authors contributed equally to this work.
* dtwhite@clarkson.edu

Abstract

Retinal detachment (RD) is the separation of the neural layer from the retinal pigmented epithelium thereby preventing the supply of nutrients to the cells within the neural layer of the retina. In vertebrates, primary photoreceptor cells consisting of rods and cones undergo daily renewal of their outer segment through the addition of disc-like structures and shedding of these discs at their distal end. When the retina detaches, the outer segment of these cells begins to degenerate and, if surgical procedures for reattachment are not done promptly, the cells can die and lead to blindness. The precise effect of RD on the renewal process is not well understood. Additionally, a time frame within which reattachment of the retina can restore proper photoreceptor cell function is not known. Focusing on rod cells, we propose a mathematical model to clarify the influence of retinal detachment on the renewal process. Our model simulation and analysis suggest that RD stops or significantly reduces the formation of new discs and that an alternative removal mechanism is needed to explain the observed degeneration during RD. Sensitivity analysis of our model parameters points to the disc removal rate as the key regulator of the critical time within which retinal reattachment can restore proper photoreceptor cell function.

Introduction

The retina is the part of the eye containing photoreceptor cells [1]. In vertebrates, photoreceptor cells are classified into two, rods and cones [2]. Structurally, rod and cone cells have outer segment (OS), inner segment (IS), cell body, and synaptic terminals [3] (see Fig 1A). The OS of these cells is filled with tiny membranous discs harboring visual pigment molecules responsible for capturing and converting light energy into electrical signals perceived by the brain to enable vision [4–9]. Rod and cone cells differ in the shape of their OS, in functionality, and the nature of the discs comprising their OS. Morphologically, the cone OS has a cone-like shape with continuous discs connected to the OS cell membrane and are opened to the extracellular space. Cones are less sensitive to light and are responsible for color vision. On the other hand, rod cells have a cylindrical OS, with discrete discs that are separated from each other and the surrounding plasma membrane. They are highly sensitive to light and are responsible for night vision [3, 10]. The retina has two main layers, namely, the retinal pigmented epithelium (RPE) and the neural layer (NL). The NL of the retina contains the photoreceptor cells as well as bipolar, horizontal, amacrine, ganglion, and muller

glial cells which work together to transmit signals to the brain to enable vision [11]. The RPE is a single-layer epithelium tightly joined to form a barrier between the retina and the choroid, a vascular structure surrounding the retina that supplies nutrients to the inner part of the eye and aids in thermoregulation [12]. The RPE contains lysosomes which break down discs that are shed from the rod and cone OS. It contains a dark pigment known as melanin which absorbs extra rays of light that can blur image formation and also prevents blood from entering the inner part of the eye [11].

Rods and cones undergo daily renewal of their OS through the addition of new discs at their base and the shedding of older discs from their distal ends to prevent accumulation of toxins caused by photo-oxidative compounds [13, 14]. Retinal detachment (RD), a separation of the NL from the RPE disrupts this normal renewal process. Factors such as old age, eye inflammatory diseases, tumors in the eye, or injury/trauma to the eye can cause the retina to detach [15–18]. When the retina detaches, the photoreceptor OS begins to degenerate/shorten [19, 20], yet the dynamics of this shortening are not well understood. For instance, some studies suggest that RD affects the renewal process by halting disc addition at the base of the OS [19] whereas other studies suggest that the addition of new disks continues during RD [16, 21]. It is however well established that shedding, as understood by the engulfment of discs by the RPE, stops during RD due to the separation of the NL from the RPE [19, 20]. The photoreceptor cells in a detached retina die after a certain period [16, 17, 21–23], however, if RD is treated on time, and the retina is reattached to the RPE, the possibility of rod and cone cell regeneration, and hence restoration of vision is high. Currently, the time frame within which retinal reattachment must be performed to restore vision is unknown [23].

To our knowledge, there are no mathematical models that explore the dynamics of the photoreceptor OS renewal during RD. Here, we extend the mathematical model we developed to study the normal dynamics of rod outer segment (ROS) renewal [24] to investigate the effect of retinal detachment on the renewal process. We focus our study on rod cells since the discrete nature of discs in rods, as opposed to the continuous nature of discs in cones, makes it easy to track the location of discs over time. Such tracking enables the estimation of the length of the ROS for validating mathematical models (as explained in Section Conversion from disk number to length). Another reason to study rod cells is that the survival of cone cells depends on a certain type of protein known as rod-derived cone viability factor (RdCVF) produced by rod cells [25]. It is typically the rod cells that degenerate first when the retina detaches, followed by cone cells [25, 26]. Also, the effect of RD on cone cells is similar to that of rod cells.

Our model simulations and analysis suggest that when the retina detaches, formation of new discs completely ceases or is significantly reduced. Our results further suggest that some disposal mechanism for discs must exist even though the normal shedding and disposal process is completely disrupted due to the separation of the RPE from the NL. Since the ROS continues to degenerate during RD and eventually dies after some time, by setting a critical length L_c below which the death of rod cells occurs, our model predicts the survival time for a rod cell in a detached retina which gives the time frame within which retinal reattachment can restore vision. This time frame is found to be dependent on the disc removal mechanism. Finally, we identify a range of disc addition and removal rates that can result in cell death during RD.

Mathematical model for ROS renewal

The first and only mathematical model developed to study the normal dynamics of ROS renewal, given by equations (1)-(3), is comprised of a system of ODEs that describes the

time evolution of discs in various compartments of the ROS [24].

$$\frac{dG}{dt} = \mu_g(G, M, S) - \alpha_g G \quad (1)$$

$$\frac{dM}{dt} = \alpha_g G - \alpha_s M \quad (2)$$

$$\frac{dS}{dt} = \alpha_s M - \mu_s S \quad (3)$$

That is, the ROS discs are classified into three compartments: growth (G), mature (M), and shed (S). The growth compartment is located at the very base of the ROS. Discs in this compartment are still connected to the cell membrane, where they are open to the extracellular space and have not attained full disc diameter [27–29]. We assume that new discs are added to the G compartment at a disc addition rate μ_g, which describes the average number of discs added to the ROS each day. The mature compartment (M) is located above the growth compartment and consists of fully developed discs detached from the OS cell membrane. We assume that discs from the G compartment mature into the M compartment at the rate α_g. This rate is governed by the rate of translocation of discs along the ROS. The discs are then shed from the mature compartment to the shed compartment at the shedding rate α_s, being engulfed by the RPE. Finally, shed discs are disposed of by the RPE at disposal rate μ_s.

Fig 1. Rod cell and compartmental diagram. A shows the four main parts of a rod cell, namely the rod outer segment (ROS), inner segment, cell body and the synaptic terminal. In addition, we highlight the RPE where shed discs are disposed of. The categorization of discs in various compartments is also shown. **B** shows the transition of discs from one compartment (growth, mature and shed) to another. Discs are added to the G compartment at rate μ_g, they mature to the M compartment at rate α_g, are shed from the M compartment at rate α_s, and are disposed of in the S compartment at rate μ_s.

Figure 1A shows the location of discs in each of the three compartments along the ROS, while Figure 1B is a compartmental diagram showing the transition of discs from one compartment to the other.

Model assumptions

To explore the effects of RD on ROS dynamics, the original model proposed by the authors in [24] is expanded. In particular, to develop equations (1)-(3), the following assumptions for **normal ROS dynamics** were made:

1. The total length of the ROS constitutes only discs in the G and M compartments.
2. The number of discs in the ROS (i.e., $G+M$) cannot exceed some upper bound D_{max}. We assume this since the retina has a finite thickness such that ROS cannot grow without bound.
3. New discs are continuously added to the base of the ROS through membrane evagination at the disc addition rate μ_g [27–29].
4. The addition of new discs is faster when the ROS is short (during development), and slows down as the ROS approaches the maximum length (i.e., $G + M \to D_{max}$) [3]. As such, we define the rate of addition of new discs to be

$$\mu_g(G, M, S) = \mu_0 \frac{D_{max}}{G + M} \quad (4)$$

where μ_0 is the minimum rate of addition of new discs.

5. Shed discs in the RPE are disposed of at the rate μ_s. Although the exact disposal rate has not been quantified experimentally, it is a biological process that is known to occur [30]. Our mathematical model requires this disposal term so that the number of discs in the S compartment does not become too large.
To account for RD, we make the following two assumptions:

6. Normal shedding, as defined to be the engulfment of discs at the distal end by the RPE [31], cannot exist during RD due to the separation of the RPE from the NL [20]. Since disc addition and shedding are the only two processes known to control the ROS length [32], the observed degeneration/shortening of the ROS during RD suggests the existence of some removal and disposal mechanism of ROS discs. To account for this removal process during RD, we multiply the shedding rate α_s by a dimensionless parameter

$$\gamma(t) = \begin{cases} \gamma_0 & T_0 \leq t < T_a \\ 1.0 & t \geq T_a \end{cases} \tag{5}$$

where $T_0 = 0$ is the time of retinal detachment and $t = T_a$ is the time of retinal reattachment as illustrated in Fig 2A. We assume that this parameter works to either increase, decrease, or keep fixed, the normal removal rate of discs. We assume this since there is no experimental data on such an alternative removal process. That is, we assume $\gamma_0 \in [0, 2]$ such that the alternative removal rate during RD is either less than ($\gamma_0 \in [0, 1)$), equal to ($\gamma_0 = 1$), or greater than ($\gamma_0 \in (1, 2]$) the normal shedding rate.

7. RD prevents the supply of nutrients to the cells within the NL of the retina [33]. To capture the effect of RD on the addition of new discs at the base of the ROS, we assume that when the NL of the retina is detached from the RPE, the addition of new discs at the base is reduced by a certain factor due to the lack of supply of nutrients to the affected cells. In particular, we let

$$\delta(t) = \begin{cases} \delta_0 & T_0 \leq t < T_a \\ 1.0 & t \geq T_a \end{cases} \tag{6}$$

where $\delta_0 \in [0, 1]$, as shown in Fig 2B, describes the severity of RD on the addition of new discs.

Fig 2. Step functions gamma and delta. Illustration for functions $\gamma(t)$ (which affects disc removal rate) and $\delta(t)$ (which affects the discs addition rate), that take on values $\gamma_0 \in [0, 2]$ and $\delta_0 \in [0, 1)$ respectively, during RD. Setting both parameters equal to 1.0 signifies normal cell behavior, and hence reattachment of the retina to the RPE at the time T_a, (here 120 days).

With the above-stated assumptions, and using the compartmental diagram shown in Figure 1B, the model we developed to help provide clarity to the precise effect of retinal detachment on the renewal of ROS is given by

$$\frac{dG}{dt} = \mu_0 \frac{\delta D_{max}}{G + M} - \alpha_g G \tag{7}$$

$$\frac{dM}{dt} = \alpha_g G - \gamma \alpha_s M \tag{8}$$

$$\frac{dS}{dt} = \gamma \alpha_s M - \mu_s S \tag{9}$$

Conversion from disk number to length

Experiments have been developed to measure ROS renewal dynamics in terms of ROS length [24]. Here we describe a method for converting disc number to length, which can help to compare our simulation results with experiments. As stated above in the model assumption, the total length of the ROS is proportional to the number of discs in the G and M compartments. As shown in Figure 1A, we let Δ_T be the average thickness of a disc and Δ_s the average disc-disc spacing. Then the approximate length of the ROS with N discs at anytime t (ie $N(t) = G(t) + M(t)$) is given by

$$L(t) = \Delta_T N(t) + \Delta_s[N(t) - 1]. \tag{10}$$

On the other hand, knowing the length $L(t)$ of the ROS at any time t, we can estimate the number of discs using the relation

$$N(t) = \frac{L(t) + \Delta_s}{(\Delta_s + \Delta_T)}. \tag{11}$$

With the above relations, we perform simulations using the length associated with each of the three compartments. Going forward, we will denote the length associated with the number of discs in the G, M and S compartments by $\hat{L}_g$, $\hat{L}_m$ and $\hat{L}_s$ respectively. Therefore in terms of length, the model describing the renewal of ROS during RD is

$$\frac{d\hat{L}_g}{dt} = \mu_0 \frac{\delta L_{max}}{\hat{L}_g + \hat{L}_m} - \alpha_g \hat{L}_g \tag{12}$$

$$\frac{d\hat{L}_m}{dt} = \alpha_g \hat{L}_g - \gamma \alpha_s \hat{L}_m \tag{13}$$

$$\frac{d\hat{L}_s}{dt} = \gamma \alpha_s \hat{L}_m - \mu_s \hat{L}_s \tag{14}$$

where L_{max} is the maximum length any ROS can attain and relates to the maximum disc number D_{max} by

$$L_{max} = \Delta_T D_{max} + \Delta_s (D_{max} - 1) \tag{15}$$

In simulating the model, we assume an initial condition of $(G_0, M_0, S_0) = (94, 627, 157)$ discs, which corresponds to initial lengths $(\hat{L}_{g_0}, \hat{L}_{m_0}, \hat{L}_{s_0}) \approx (3, 20, 5)\mu m$ for mice. In addition, we assume that the initial time corresponds to the time of RD (if it occurs) and that the maximum length any mice ROS can attain is $L_{max} = 30\mu m$ which in terms of disc numbers corresponds to $D_{max} \approx 940$ discs. We choose this maximum value because the average length of mice ROS has been reported to be $23.8\mu m$ [34] and that of Royal College of Surgeons (RCS) rats to be $22.7 \pm 2.4\mu m$ [35]. Table 1 lists the parameter values and references, as well as the units for the state variables and parameters.

Equilibrium and stability analysis

We start our model analysis by finding the equilibrium point(s) of the system. This will help us explore the long-term behavior/length of the ROS during retinal detachment. Since the ROS continuously degenerates during retinal detachment, we assume that there exists a critical length (L_c) below which the rod cell dies. The equilibrium point(s) can help us determine whether or not the ROS length will eventually fall below this critical length. Before determining the equilibrium point(s) of the system and its stability, we first reduce the number of parameters in the model by nondimensionalizing

Table 1. Parameter values

Quantity	Value	Unit
$\hat{L}_g, \hat{L}_m, \& \hat{L}_s$	-	μm
G, M, S	-	discs
Δ_T	1.638×10^{-2}	μm [34]
Δ_s	1.556×10^{-2}	μm [34]
μ_0	2.2	$\mu m/day$ [35]
α_g	0.85	$[1/day]$ [24]
α_s	0.155	$[1/day]$ estimated in this paper
μ_s	0.3	$[1/day]$ estimated in this paper
δ	$[0, 1]$	No unit
γ	$[0, 2]$	No unit

The table shows parameter values used in our simulation. The values for Δ_T and Δ_s correspond to those for mice [34]. The value for μ_0 corresponds to RCS rat [35], the value for α_g was obtained from a study of zebrafish rods [24], while the remaining parameters α_s and μ_s were obtained through a parameter sweep where the model output (length of mature ROS) was compared to experimental data from mice [34].

the system. We scale the length associated with each of the three compartments (equations (12) - (14)) by L_{max} and time by α_g^{-1} such that $L_g = \frac{\hat{L}_g}{L_{max}}$, $L_m = \frac{\hat{L}_m}{L_{max}}$, $L_s = \frac{\hat{L}_s}{L_{max}}$ and $\tau = \alpha_g t$, and arrive at

$$\frac{dL_g}{d\tau} = \bar{\mu}_0 \frac{\delta}{L_g + L_m} - L_g \quad (16)$$

$$\frac{dL_m}{d\tau} = L_g - \gamma\bar{\alpha}_s L_m \quad (17)$$

$$\frac{dL_s}{d\tau} = \gamma\bar{\alpha}_s L_m - \bar{\mu}_s L_s \quad (18)$$

where $\bar{\mu}_0 = \frac{\mu_0}{\alpha_g L_{max}}$, $\bar{\alpha}_s = \frac{\alpha_s}{\alpha_g}$ and $\bar{\mu}_s = \frac{\mu_s}{\alpha_g}$. Setting the time derivatives in equations (16)-(18) equal to zero, we arrive at 2 equilibrium points $E_{1,2} = (L_g^*, L_m^*, L_s^*)$ when $\delta \neq 0$, and a single trivial equilibrium E_0 when $\delta = 0$. That is, for $\delta \neq 0$, the equilibrium points are given by

$$E_1 = \left(\gamma\bar{\alpha}_s\sqrt{\frac{\bar{\mu}_0\delta}{\gamma\bar{\alpha}_s(\gamma\bar{\alpha}_s+1)}}, \sqrt{\frac{\bar{\mu}_0\delta}{\gamma\bar{\alpha}_s(\gamma\bar{\alpha}_s+1)}}, \frac{\gamma\bar{\alpha}_s}{\bar{\mu}_s}\sqrt{\frac{\bar{\mu}_0\delta}{\gamma\bar{\alpha}_s(\gamma\bar{\alpha}_s+1)}}\right) \quad (19)$$

$$E_2 = -\left(\gamma\bar{\alpha}_s\sqrt{\frac{\bar{\mu}_0\delta}{\gamma\bar{\alpha}_s(\gamma\bar{\alpha}_s+1)}}, \sqrt{\frac{\bar{\mu}_0\delta}{\gamma\bar{\alpha}_s(\gamma\bar{\alpha}_s+1)}}, \frac{\gamma\bar{\alpha}_s}{\bar{\mu}_s}\sqrt{\frac{\bar{\mu}_0\delta}{\gamma\bar{\alpha}_s(\gamma\bar{\alpha}_s+1)}}\right). \quad (20)$$

The equilibrium point E_2 is not biologically feasible because each of the three state variables (L_g, L_m and Ł$_s$) corresponds to a non-negative length. When $\delta = 0$, the two equilibrium points E_1 and E_2 coalesce into E_0 such that

$$E_0 = (0, 0, 0). \quad (21)$$

Stability of the equilibrium point(s)

To determine the stability of the equilibrium points, we compute the Jacobian of the system defined by equations (16)-(18) which gives

$$J(L_g, L_m, L_s) = \begin{pmatrix} -\frac{\delta\bar{\mu}_0}{(L_g+L_m)^2} - 1 & -\frac{\delta\bar{\mu}_0}{(L_g+L_m)^2} & 0 \\ 1 & -\gamma\bar{\alpha}_s & 0 \\ 0 & \gamma\bar{\alpha}_s & -\bar{\mu}_s \end{pmatrix}. \quad (22)$$

When $\delta \neq 0$ (i.e., making a substitution of E_1 and then E_2 into the Jacobian), the characteristic polynomial $P_{1,2}(\lambda)$ corresponding to the equilibrium points E_1 and E_2 is given by

$$P_{1,2}(\lambda) = -(\lambda + \bar{\mu}_s)\left[\lambda^2 + (a + \gamma\bar{\alpha}_s + 1)\lambda + (a + \gamma\bar{\alpha}_s(a+1))\right], \tag{23}$$

where $a = \frac{\delta\bar{\mu}_0}{(L_g+L_m)^2} \geq 0$. The equilibrium points E_1 and E_2 have the same eigenvalues given by

$$\lambda_1 = -\bar{\mu}_s, \qquad \text{and} \tag{24}$$

$$\lambda_{2,3} = -\frac{1}{2}\left[(a + \gamma\bar{\alpha}_s + 1) \pm \sqrt{(a + \gamma\bar{\alpha}_s + 1)^2 - 4(a + \gamma\bar{\alpha}_s(a+1))}\right]. \tag{25}$$

From equation (25), we observe that the real part of the square root term, $\Re\left(\sqrt{(a + \gamma\bar{\alpha}_s + 1)^2 - 4(a + \gamma\bar{\alpha}_s(a+1))}\right) \leq (a + \gamma\bar{\alpha}_s + 1)$. Thus, all the eigenvalues corresponding to equilibria E_1 and E_2 have negative real part which means they are both globally asymptotically stable. On the other hand, if RD completely stops the formation of new disks at the base of ROS such that $\delta = 0$, the Jacobian of the system corresponding to E_0 is

$$J(E_0) = \begin{pmatrix} -1 & 0 & 0 \\ 1 & -\gamma\bar{\alpha}_s & 0 \\ 0 & \gamma\bar{\alpha}_s & -\bar{\mu}_s \end{pmatrix}, \tag{26}$$

which has eigenvalues $\lambda_1^{E_0} = -1$, $\lambda_2^{E_0} = -\gamma\bar{\alpha}_s$ and $\lambda_3^{E_0} = -\bar{\mu}_0$. Thus, for $\delta = 0$, if there is some disc removal rate such that $\gamma \neq 0$, the equilibrium point E_0 is also globally asymptotically stable. However, if $\gamma = 0$ such that there is no disc removal, the analytic solution to equations (16)-(18) is given by

$$(L_g, L_m, L_s) = (L_{g_0}e^{-t}, \quad L_{g_0} + L_{m_0} - L_{g_0}e^{-t}, \quad L_{s_0}e^{-\bar{\mu}_0 t}) \tag{27}$$

where L_{g_0}, L_{m_0} and L_{s_0} are the initial lengths corresponding to discs in the G, M and S compartments, respectively (i.e., at the time of RD).

Result and discussion

Some studies suggest that RD halts the formation of new discs at the base of the ROS [19] but others suggest the contrary [16, 21]. Shedding, as understood by the engulfment of ROS discs by the RPE, ceases during RD due to the separation of the RPE from the NL [19, 20]. The precise effect of RD on the renewal of ROS is unclear. The ROS is observed to degenerate when the retina detaches [19, 20], and photoreceptor cells in a detached retina die after a certain time [16, 17, 21–23]. Thus, the mechanism responsible for the degeneration of ROS during RD, and those that dictate the survival time of rod cells in a detached retina are unknown. Here, we present the results of our model simulation and analysis to help answer these questions and provide clarity to the competing theories regarding ROS renewal. Resolving the controversies surrounding the renewal process and understanding the precise effect of RD on the renewal of ROS can help improve the existing therapy for RD and/or help devise new treatments for RD. Investigation of the survival time of a rod cell in a detached retina provides a time frame within which RD surgery can restore vision.

Normal dynamics of a rod outer segment

Setting $\delta = 1$ and $\gamma = 1$ in equations (12)-(14), we capture the normal dynamics/renewal of a healthy ROS. Here, we simulate the dimensional version of the system, given by equations (12) to (14), to better compare our results with experiments/clinical findings. Experiments on mice, rats, and frogs show that it takes on average 9-14 days for the entire length of the ROS to be renewed [13, 26, 36]. To highlight the *normal dynamics* of the ROS using our model, we assume that there is just one disc in the G-compartment initially with no discs in both M and S compartments, representing a developing rod cell. Fig 3 shows the length dynamics of all three compartments of the ROS and the total length (in red). Here, we used the average thickness of a disc (Δ_T) and the disc-disc spacing (Δ_s) for mice [34]. The predicted time to equilibrium is approximately 14 days, which is consistent with experimental findings.

Fig 3. Normal ROS renewal. The figure shows the evolution of lengths associated with the G (blue curve), M (green curve), and S (magenta curve) compartments of a normal developing ROS, as well as the total ROS length (red curve where $L_t(t) = L_g(t) + L_m(t)$). Initial condition is $(G_0, M_0, S_0) = (1, 0, 0)$ discs which translates to $(L_{g_0}, L_{m_0}, L_{s_0}) = (0.01638, 0, 0)\mu m$ for mice. The time to equilibrium predicted by the model is approximately 14 days, consistent with experimental findings [13, 26, 36].

Reduction in addition of new discs and complete suppression of disc removal ($\delta < 1$ and $\gamma = 0$)

In general, it is observed that when the NL of the retina is detached from the RPE, the ROS degenerates/shortens [16, 19–21]. A degenerating ROS can be rescued to re-establish the equilibrium length if the NL of the retina is surgically reattached to the RPE before some **critical time** (*how long a rod cell can survive in a detached retina*) [16]. However, if the detachment lasts long enough, the rod cell might die and not be able to re-establish itself when the retina is surgically reattached to the RPE [17, 23, 37]. As stated previously, disc addition and shedding are the only two processes known to control the length of the ROS [32], and there is controversy surrounding whether or not disc addition persists or is halted. Although the normal shedding is prevented during RD due to the separation of the RPE from the NL, the observed degeneration of the ROS during RD suggests the possibility of some alternative removal mechanism. Here, we investigate whether or not disc addition can persist in the absence of an alternative removal mechanism. By setting $\gamma = 0$ to halt the disc removal process, we simulate the model for different reduced disc addition rates (i.e., $\delta \in (0, 1)$), one of which is illustrated in Fig 4. Here, we assume that the normal addition rate is reduced by 98.64% (ie $\delta = 0.0136$). Recall that the initial time of simulation corresponds to the time of RD. We observed that the ROS continuously increases in length throughout RD. We can infer from equilibrium point E_1 in equation (19) that the long-term dynamics shown in Fig 4 is true for any $\delta \in (0, 1)$). That is, since $L_t = L_g + L_m$, when $\delta \neq 0$ $\lim_{\gamma \to 0} L_t \to +\infty$ indicating that once the alternative removal is suppressed, no matter how small the addition rate is, there will be an accumulation of discs which will increase the ROS length. This dynamics contradicts the experimentally observed degeneration/shortening of ROS during RD. Thus, our result suggests that disc removal cannot be halted if disc addition persists during RD.

Fig 4. Addition without removal of discs. Illustration of the dynamics of a ROS during RD if the normal rate of addition of new discs is reduced, here by 98.64% (ie $\delta = 0.0136$) while disc removal is halted completely. We observe an increase in the length of the ROS which contradicts the observed degeneration/shortening of ROS during RD.

Halting of both addition of new discs and the removal of older discs ($\delta = 0$ and $\gamma = 0$)

It is well established that the shedding of discs into the RPE ceases during RD. However, there could be some alternative removal mechanism taking place during RD. Here, we investigate whether or not the alternative removal mechanism as well as the formation of new discs can cease during RD. By setting $\delta = 0$ and $\gamma = 0$, we assume that both the addition of new discs at the base and the removal of older discs at the top ceases when the NL of the retina is detached from the RPE. The analytic solution corresponding to this case is presented in equation (27). The phase portrait for this case is shown in Fig 5A in addition to the evolution of the total length of the ROS as well as the lengths corresponding to discs in S compartments in Fig 5B. These results show that the length of the ROS remains near-constant throughout RD. This result contradicts the experimentally observed degeneration of ROS that occurs during RD and inevitable cell death when RD is prolonged. Thus, the model suggests that the addition of new discs and the removal of older discs cannot both cease during RD.

Fig 5. Neither addition nor removal of discs. (A) is a phase portrait in $L_g - L_m$ plane and **(B)** shows trajectories for L_t&L_s as well as the critical length L_c below which rod cell death occurs. Results show that the length of the ROS remains constant if both the addition of new discs and removal of older discs cease during RD thereby contradicting the observed degeneration/shortening

Halting of addition of new discs and reduction in removal of older discs ($\delta = 0$ and $\gamma \neq 0$)

It is observed that RD leads to degeneration/shortening of the ROS and eventually cell death (ROS length falls below the critical length L_c) if detachment lasts beyond a certain time T_c. Here, we investigate whether or not RD prevents the formation of new discs but allows the removal of older discs. To do this, we set $\delta = 0$ to prevent the addition of new discs at the base of the ROS and vary $\gamma \in (0, 2)$ to allow for different removal rates. When $\delta = 0$, the two equilibrium points E_1 and E_2 coalesce into E_0 which is globally asymptotically stable. The output of our simulation, as shown in Fig 6, indicates that by halting disc addition and allowing the removal of older discs, the ROS continuously decreases in length towards zero. Thus, once the addition of new discs is halted, no matter how small the removal rate is, the ROS will eventually decrease below the threshold/critical length L_c thereby resulting in the death of rod cells. This result is consistent with the experimental finding by Kaplan, who suggests that RD inhibits the formation of discs or results in the abnormal assembly of new discs such that new discs are not able to configure themselves into the ROS [19]. Thus, our results suggest that RD completely stops the formation of new discs, a theory that is unclear in the literature as some studies suggest that disc addition persists during RD [16, 21]. In addition, since the RPE responsible for normal disc shedding is separated from the NL during RD thereby preventing the normal shedding process [19, 20], our model suggests that an alternate removal and disc disposal mechanism must exist during RD to explain the

observed degeneration/shortening of the ROS and eventual cell death for prolonged RD.

Fig 6. Removal without the addition of discs. Here the addition of new discs is halted ($\delta = 0$) and there is a 37.5% reduction ($\gamma = 0.625$) in the normal removal rate. The ROS decreases below the critical length at approximately 25 days signifying cell death

Reduction in both the addition of new discs and removal of older discs ($0 < \delta < 1$ and $0 < \gamma < 1$)

Here, we investigate the possibility of having both the addition of new discs as well as some removal mechanism at different rates during RD. Since RD prevents the supply of nutrients to the cells within the NL of the retina [33], we assume that the rate of addition of new discs cannot be more than the normal addition rate. Since no data exists on the alternative removal process, we propose that the alternative removal rate can be less than, equal to, or greater than the normal shedding rate. Varying $\delta \in (0, 1)$ and $\gamma \in (0, 2)$, we respectively capture the different rates of addition of new discs at the base and removal of older discs at the top. As shown in Fig 7A, we note that during RD, if the rate of addition of new discs is significantly low (here 0.68% of the normal addition rate) the total length of the ROS decreases below the critical length L_c thereby resulting in cell death. However, if the addition rate is at least 1.3% of the normal addition rate, the total ROS length does not fall below the critical length (*i.e., rod cell does not die*) as shown in Fig 7B. This result supports the discovery by Kaplan [19], who suggested that RD either inhibits the formation of new discs or results in abnormal assembly of discs that are not able to configure themselves into the ROS. Since the formation of new discs occurs through membrane evagination at the ROS base thereby displacing already formed discs along the ROS [3, 28, 38], abnormal assembly of discs will result in very low disc addition rate leading to cell death when detachment last long enough. Thus, the model predicts that RD leads to a significantly low addition rate with some removal mechanism. The observed low addition rate in our model simulation supports the idea of an abnormal assembly of discs during RD.

Fig 7. Formation and removal of disc. Illustration of the dynamics of a ROS during RD if both the addition of new discs and removal of older discs persist during RD (where disc addition is significantly reduced). In **(A)**, the normal rate of addition of new discs was reduced by 99.32% while the removal of older discs was increased by 87.5%. The ROS decreased below the critical length at approximately 10 days thereby resulting in cell death. In **(B)**, the normal addition rate was reduced by 98.36% while the normal shedding rate was reduced by 37.5% and the ROS did not decrease below the critical length (cell did not die).

We further determine the long-term behavior of the ROS during RD to help us predict when RD leads to eventual cell death (such that length falls below L_s). Fig 8 A, B, and C are phase portraits in the $L_g - L_m$ plane showing the stability of the equilibrium point E_1 when $\delta \neq 0$ and Fig 8D describing the phase portrait when $\delta = 0$. In all figures, we set $\gamma \neq 0$ such that some removal mechanism exists since our model simulation and analysis suggest that an alternation removal mechanism is needed to explain the observed degeneration and cell death for prolonged RD. Here we see that when $\delta \neq 0$, decreasing δ (i.e., increasing level of severity of RD on the addition of new discs), the equilibrium point E_1 moves closer to the origin where the total ROS length gets smaller but never reaches zero. Thus, if the formation of new discs persists during RD, the ROS cannot completely degenerate (i.e., ROS length cannot decrease to zero). However,

depending on the rate of formation of new discs and the critical length L_c below which the cell can not survive, the ROS length may or may not fall below this critical length. When $\delta = 0$, the two equilibrium points E_1 and E_2 coalesce to form a stable equilibrium point E_0 at the origin. This means that no matter how small the critical length is, once formation of new discs ceases during RD, the ROS will always fall below the critical length signifying cell death if some removal mechanism of ROS disc exists.

Fig 8. Phase plot. Phase portraits for varying disc addition rate $\delta\mu_0$ illustrating the effect of RD. Panel **A** shows a phase portrait for normal ROS dynamics ($\delta = 1$ and $\gamma = 1$), panels **B** and **C** show an example of phase portraits during RD where we reduce the disc addition rate but keep the disc removal fixed ($\delta < 1$ and $\gamma = 1$), and panel **D** illustrates a phase portrait when RD halts the addition of new discs ($\delta = 0$).

Criteria for unconditional ROS regeneration

Our model simulation and analysis results suggest that, for the ROS to shorten during RD, falling below some critical length L_c at critical time T_c, **the rate of disk addition must be zero or close to it, and some disc removal mechanism must exist**. Here, we determine the range of values for the disc addition rate ($\nu = \delta\mu_0$) and removal rate ($\varepsilon = \gamma\alpha_s$) that can eventually drive the ROS below the critical length L_C. As detailed in appendix S1 Appendix, the ROS length will fall below L_C if the addition and the removal rates satisfy the inequalities given by

$$\nu < \kappa \quad \text{and} \quad \varepsilon > \frac{\alpha_g \nu}{\kappa - \nu} \tag{28}$$

which we represent by the unshaded portion in Fig 9. This portion decreases or increases as we shift the vertical line $\nu = \kappa$ to the left or right respectively, where $\kappa = \frac{\alpha_g L_c^2}{L_{max}}$. This result suggests that the size of the unshaded region is controlled by the critical length L_c and the disc addition rate α_g such that the smaller L_c, the smaller the unshaded region, and vice versa. This means that the possibility of rod cell death is high if the critical length is large. The ROS will always regenerate upon reattachment of the RPE to the NL if the addition and removal rates satisfy the inequalities

$$\nu \geq \kappa \tag{29}$$

or

$$\nu < \kappa \quad \text{and} \quad \varepsilon \leq \frac{\alpha_g \nu}{\kappa - \nu}, \tag{30}$$

where the shaded portion in Fig 9 represents the range of values for the disc addition and removal rates for which the ROS remains above the critical length.

Fig 9. Domain for cell death. The unshaded portion labeled A in the figure shows the domain for the addition of new discs ($\nu = \delta\mu_0$) and the removal of older discs ($\varepsilon = \gamma\alpha_s$) during RD that will eventually drive the ROS length below the critical length leading to cell death. In the shaded region labeled B, the length of the ROS will always remain above the critical length L_c, thus the rod cell cannot die and reattachment at any time will result in regeneration.

Critical time to cell death

The recovery of sight after RD surgery depends on how long the retina has been detached [39, 40]. Here we investigate the time frame within which RD surgery can

restore vision such that the length of the ROS is above the critical length L_C. Biologically, this time frame corresponds to how long the photoreceptor (rod) cell can survive when the retina detaches. We investigate how the various parameters in the model influence the critical time T_C (the time at which the ROS falls below L_C). We find that T_C depends on the disc removal rate such that the greater the removal rate, the smaller the critical time and vice versa. Thus if the removal rate during RD is higher than the normal shedding rate the critical time for reattachment is small. Fixing all other parameters (i.e., fixing $\mu_0, \alpha_g, \alpha_s, \mu_s$, and setting $\delta = 0$) and varying the disc removal rate by varying $\gamma \in [0, 2]$, Fig 10A shows how the critical times T_C varies. We observe that the T_C is more sensitive if $\gamma \in [0, 0.5]$ but less sensitive if $\gamma \in (0.5, 2]$. In particular, there are large changes for the critical time for small changes in γ when $\gamma < 0.5$. For $\gamma > 0.5$, the critical time is small and changes only slightly as γ is increased. Similar analysis done for the maturation rate α_g, as shown in Fig 10B, reveals that the critical time changes slightly when the disc maturation rate is small ($\alpha_g < 0.34$) but has no effect on the critical time when the disc maturation rate is high ($\alpha_g \geq 0.34$). Figure Fig 10C, illustrates that the critical time is independent of variations in the disposal rate μ_s, such that the critical time remains fixed. Based on these observations, the model suggests that the critical time at which the ROS can no longer regenerate is dependent and highly sensitive to changes in disc removal such that when γ is small the critical time is high but varies significantly for small perturbations in γ. For γ high, the critical time is small and varies only slightly for changes in γ. As the removal mechanism for discs during RD is not well understood (i.e., we do not know whether the removal rate is greater, equal to, or smaller than the shedding rate in normal ROS), our modeling results illustrate the need for better biological understanding of the disc removal process during RD so that we might establish the time frame within which RD surgery can successfully restore vision.

Fig 10. Sensitivity plot. The figure shows the dependence of the critical time on γ, α_g and μ_s. In **A**, increasing γ (ie increasing the removal rate) decreases the critical time. In **B**, when $\alpha_g \in [0, 0.34)$ the critical time decreases with increasing α_g (*not as much as* γ) but does not affect the critical time when $\gamma \geq 0.34$. In **C**, the disposal rate does not affect the critical time.

Conclusion

Fig 11. Proposed compartmental diagram. The figure illustrates a proposed mechanism that likely occurs during RD. The normal shedding as understood by the engulfment of discs at the distal end of the ROS by the RPE does not exist during RD due to the separation of the RPE from the NL. $\varepsilon = \gamma\alpha_s$ is the proposed alternative removal rate of discs from the ROS during RD and μ_r the disposal rate.

We developed a mathematical model to describe the renewal process of ROS during RD. Using the output of our simulation, we were able to test competing hypotheses about the effect of RD on the addition of discs to the ROS. Our model suggests that disc addition is either halted or significantly reduced during RD [19]. Since we know that shedding, as defined in normal cells, can not occur as the RPE is removed from the NL [19, 20], our model also suggests that another removal and disposal mechanism must exist to get rid of discs at the distal end of the ROS to explain the observed ROS degeneration. Fig 11 describes our new idea (our modeling results) for how discs evolve in the ROS during RD (the old model is shown in red, the new is shown in black),

where $\varepsilon = \gamma\alpha_s$ represents the alternative disc removal rate during RD and μ_r describes a disposal rate. In addition to studying the effect of RD on the renewal process of the ROS, we also examined the time (the critical time T_C) it takes for the ROS to decrease below a critical length L_C (which we assume results in cell death). As shown in Fig 10, we observed that the critical time is dependent on the rate at which ROS discs are removed, such that this time is very sensitive when $\gamma < 0.5$ but less sensitive when $\gamma \geq 0.5$. Since we do not know if the removal rate is larger ($\gamma > 1$), equal to ($\gamma = 1$), or smaller than ($\gamma < 1$) the disc shedding rate in normal ROS. We also provided a quantitative description of how changes in the disc addition rate and the removal rate lead to eventual cell death during retinal detachment (the result is shown in Fig 10). This result indicates that the parameter ranges depend on the critical length (L_c) below which cell death occurs and the maturation rate α_g. This work sets the premise for a further experimental investigation into the threshold/critical length below which photoreceptor cells die, as well as the removal and disposal mechanisms of ROS discs during RD. Once these are established, the model can aid surgeons in understanding an approximate time frame or *window of opportunity* for which RD surgery will be successful.

The model proposed here is one of the first mathematical modeling frameworks to describe ROS dynamics during RD, where the authors have also used this modeling framework in [24] to describe the normal renewal process. As such, the modeling work completed here will be valuable in understanding other questions surrounding the ROS renewal process. In future work, we hope to look at extensions of this model to account for more complicated relations between the disc addition and shedding machinery as well as other factors regulating the renewal process. For example, we know that shedding is affected by the light-dark cycle [36, 41–44] and concentrations of certain chemicals such as dopamine and melatonin [45–47].

Acknowledgments

This research was funded by the National Science Foundation under the Grant MCB-1951453. The authors would like to thank Dr. Abigail Jensen (UMass Amherst Biology Department) for engaging in helpful discussions that led to some important modeling considerations.

Declaration of interest: none

Supporting information

S1 Appendix.

Ranges for addition and removal rates that can lead to cell death

Retinal detachment leads to shortening of the ROS [48] and eventual cell death for prolonged detachment [39]. We assume that, for a rod cell in a detached retina whose outer segment (OS) is shortening, there exists a minimum length below which the rod cell is unable to survive, which we refer to as the critical length and denote by L_c. Here, we determine the range of values for the removal rate ($\gamma\alpha_s$) and the addition rate ($\delta\mu_0$) during RD that can drive the ROS below the critical length L_c, leading to cell death.

For simplicity in notation, we denote the addition rate by $\nu = \delta\mu_0$ and the removal rate by $\varepsilon = \gamma\alpha_s$ and let $\hat{L}_T(t)$ be the length of the ROS at any time t. Then, by adding the L_g and L_m components of the feasible equilibrium point E_1 in equation (19), the equilibrium (total) length of the ROS is given by

$$L_T^* = (\gamma\bar{\alpha}_s + 1)\sqrt{\frac{\bar{\mu}_0\delta}{\gamma\bar{\alpha}_s(\gamma\bar{\alpha}_s + 1)}} \tag{31}$$

where $L_T^* = \frac{\hat{L}_T}{L_{max}}$ is a dimensionless quantity representing the total length of the ROS. For cell death to occur, we must have this length fall below the critical value such that

$$\hat{L}_T < L_c \implies L_T^* < \frac{L_c}{L_{max}} \tag{32}$$

Substituting equation (31) into (32), squaring both sides and simplifying we arrive at

$$\bar{\mu}_0\delta(\gamma\bar{\alpha}_s + 1) < \gamma\bar{\alpha}_s\frac{L_c^2}{L_{max}^2} \tag{33}$$

Recall from Section Equilibrium and stability analysis that $\bar{\mu}_0 = \frac{\mu_0}{\alpha_g L_{max}}$ and $\bar{\alpha}_s = \frac{\alpha_s}{\alpha_g}$. Substituting these into inequality (33) and simplifying gives

$$\mu_0\delta(\gamma\alpha_s + \alpha_g) < \gamma\alpha_s\frac{\alpha_g L_c^2}{L_{max}}. \tag{34}$$

Denoting $\kappa = \frac{\alpha_g L_c^2}{L_{max}}$ in inequality (34), we get

$$\varepsilon(\nu - \kappa) < -\alpha_g\nu, \tag{35}$$

an inequality describing the relationship between disc addition and removal such that, if satisfied, will lead to rod cell death (i.e., total ROS length will eventually fall below the critical length L_c). Since $\varepsilon, \nu, \kappa, \alpha_g$ are all non-negative, inequality (35) holds only when

$$\nu < \kappa \quad \text{and} \quad \varepsilon > \frac{\alpha_g\nu}{\kappa - \nu} \tag{36}$$

Fig 9 illustrates regions in $\nu\varepsilon$-plane where the ROS will eventually fall below the critical length L_c signifying rod cell death or can not fall below L_c no matter how long the detachment lasts. In particular, if the rate of addition of new discs ($\nu = \delta\mu_0$) and removal of older discs ($\varepsilon = \gamma\alpha_s$) during RD satisfies the inequality in (36) (ie ν and ε falls within the unshaded portion of Fig 9), the ROS will eventually decrease below the critical length (L_c) leading to cell death. On the other hand, if

$$\nu \geq \kappa \tag{37}$$

or

$$\nu < \kappa \quad \text{and} \quad \varepsilon \leq \frac{\alpha_g\nu}{\kappa - \nu} \tag{38}$$

the ROS cannot decrease below the critical length L_c. This means if the removal and addition rates of discs during RD fall within the shaded portion of Fig 9, the rod cell cannot die no matter how long RD lasts

References

1. Morshedian A, Fain GL. The evolution of rod photoreceptors. Philosophical Transactions of the Royal Society B: Biological Sciences. 2017;372(1717):20160074.

2. Verasztó C, Gühmann M, Jia H, Rajan VBV, Bezares-Calderón LA, Pineiro-Lopez C, et al. Ciliary and rhabdomeric photoreceptor-cell circuits form a spectral depth gauge in marine zooplankton. Elife. 2018;7:e36440.

3. Fu Y, Yau KW. Phototransduction in mouse rods and cones. Pflügers Archiv-European Journal of Physiology. 2007;454:805–819.

4. Kolb H, Fernandez E, Nelson R. Webvision: the organization of the retina and visual system [Internet]. 1995;.

5. Isayama T, Zimmerman AL, Makino CL. The molecular design of visual transduction; 2009. Available from: `https://www.biophysics.org/Portals/0/BPSAssets/Articles/Phototransduction.pdf`.

6. Jonnal RS, Besecker JR, Derby JC, Kocaoglu OP, Cense B, Gao W, et al. Imaging outer segment renewal in living human cone photoreceptors. Optics express. 2010;18(5):5257–5270.

7. Campbell LJ, West MC, Jensen AM. A high content, small molecule screen identifies candidate molecular pathways that regulate rod photoreceptor outer segment renewal. Scientific Reports. 2018;8(1):1–15.

8. Campbell LJ, Jensen AM. Phosphodiesterase inhibitors sildenafil and vardenafil reduce zebrafish rod photoreceptor outer segment shedding. Investigative ophthalmology & visual science. 2017;58(13):5604–5615.

9. Mazzolini M, Facchetti G, Andolfi L, Proietti Zaccaria R, Tuccio S, Treu J, et al. The phototransduction machinery in the rod outer segment has a strong efficacy gradient. Proceedings of the National Academy of Sciences. 2015;112(20):E2715–E2724.

10. Spencer WJ, Lewis TR, Pearring JN, Arshavsky VY. Photoreceptor discs: built like ectosomes. Trends in cell biology. 2020;30(11):904–915.

11. Mahabadi N, Al Khalili Y. Neuroanatomy, retina. In: StatPearls [Internet]. StatPearls Publishing; 2021.Available from: `https://www.ncbi.nlm.nih.gov/books/NBK545310/`.

12. Nickla DL, Wallman J. The multifunctional choroid. Progress in retinal and eye research. 2010;29(2):144–168.

13. LaVail MM. Photoreceptor characteristics in congenic strains of RCS rats. Investigative ophthalmology & visual science. 1981;20(5):671–675.

14. Bassi C, Powers M. Shedding of rod outer segments is light-driven in goldfish. Investigative ophthalmology & visual science. 1990;31(11):2314–2319.

15. Erickson PA, Fisher SK, Anderson DH, Stern W, Borgula GA. Retinal detachment in the cat: the outer nuclear and outer plexiform layers. Investigative ophthalmology & visual science. 1983;24(7):927–942.

16. Guérin CJ, Lewis GP, Fisher SK, Anderson DH. Recovery of photoreceptor outer segment length and analysis of membrane assembly rates in regenerating primate photoreceptor outer segments. Investigative ophthalmology & visual science. 1993;34(1):175–183.

17. Amemiya T, Yoshida H, Harayama K, Miki M, Koizumi K. Long-term results of retinal detachment surgery. Ophthalmologica Journal International d'ophtalmologie International Journal of ophthalmology Zeitschrift fur Augenheilkunde. 1978;177(2):64–69.

18. Miller JR, Hanumunthadu D. Inflammatory eye disease: An overview of clinical presentation and management. Clinical Medicine. 2022;22(2):100.

19. Kaplan MW, Iwata RT, Sterrett C. Retinal detachment prevents normal assembly of disk membranes in vitro. Investigative ophthalmology & visual science. 1990;31(1):1–8.

20. Williams DS, Fisher S. Prevention of rod disk shedding by detachment from the retinal pigment epithelium. Investigative ophthalmology & visual science. 1987;28(1):184–187.

21. Lewis GP, Erickson PA, Anderson DH, Fisher SK. Opsin distribution and protein incorporation in photoreceptors after experimental retinal detachment. Experimental eye research. 1991;53(5):629–640.

22. Rex TS, Fariss RN, Lewis GP, Linberg KA, Sokal I, Fisher SK. A survey of molecular expression by photoreceptors after experimental retinal detachment. Investigative ophthalmology & visual science. 2002;43(4):1234–1247.

23. Burton TC. Recovery of visual acuity after retinal detachment involving the macula. Transactions of the American Ophthalmological Society. 1982;80:475.

24. Jensen AM, White D, Annan W, Gilliam L, Willoughby JJ. Overexpression of Rheb, a positive Tor regulator, reveals principles of rod outer segment size control. bioRxiv. 2023; p. 2023–09.

25. Léveillard T, Mohand-Saïd S, Lorentz O, Hicks D, Fintz AC, Clérin E, et al. Identification and characterization of rod-derived cone viability factor. Nature genetics. 2004;36(7):755–759.

26. Camacho ET, Vélez MAC, Hernández DJ, Bernier UR, Van Laarhoven J, Wirkus S. A mathematical model for photoreceptor interactions. Journal of theoretical biology. 2010;267(4):638–646.

27. Burgoyne T, Meschede IP, Burden JJ, Bailly M, Seabra MC, Futter CE. Rod disc renewal occurs by evagination of the ciliary plasma membrane that makes cadherin-based contacts with the inner segment. Proceedings of the National Academy of Sciences. 2015;112(52):15922–15927.

28. Ding JD, Salinas RY, Arshavsky VY. Discs of mammalian rod photoreceptors form through the membrane evagination mechanism. Journal of Cell Biology. 2015;211(3):495–502.

29. Besharse JC, Hollyfield JG. Renewal of normal and degenerating photoreceptor outer segments in the Ozark cave salamander. Journal of Experimental Zoology. 1976;198(3):287–301.

30. Kwon W, Freeman SA. Phagocytosis by the retinal pigment epithelium: recognition, resolution, recycling. Frontiers in immunology. 2020;11:604205.

31. Kocaoglu OP, Liu Z, Zhang F, Kurokawa K, Jonnal RS, Miller DT. Photoreceptor disc shedding in the living human eye. Biomedical optics express. 2016;7(11):4554–4568.

32. Schremser JL, Williams TP. Rod outer segment (ROS) renewal as a mechanism for adaptation to a new intensity environment. II. Rhodopsin synthesis and packing density. Experimental eye research. 1995;61(1):25–32.

33. Jalali S. Retinal detachment. Community Eye Health. 2003;16(46):25.

34. Gilliam JC, Chang JT, Sandoval IM, Zhang Y, Li T, Pittler SJ, et al. Three-dimensional architecture of the rod sensory cilium and its disruption in retinal neurodegeneration. Cell. 2012;151(5):1029–1041.

35. Lavail MM, Li L, Turner JE, Yasumura D. Retinal pigment epithelial cell transplantation in RCS rats: normal metabolism in rescued photoreceptors. Experimental Eye Research. 1992;55(4):555–562.

36. Young RW. The renewal of photoreceptor cell outer segments. The Journal of cell biology. 1967;33(1):61–72.

37. Cook B, Lewis GP, Fisher SK, Adler R. Apoptotic photoreceptor degeneration in experimental retinal detachment. Investigative ophthalmology & visual science. 1995;36(6):990–996.

38. Spencer WJ, Lewis TR, Phan S, Cady MA, Serebrovskaya EO, Schneider NF, et al. Photoreceptor disc membranes are formed through an Arp2/3-dependent lamellipodium-like mechanism. Proceedings of the National Academy of Sciences. 2019;116(52):27043–27052.

39. Faude F, Francke M, Makarov F, Schuck J, Gärtner U, Reichelt W, et al. Experimental retinal detachment causes widespread and multilayered degeneration in rabbit retina. Journal of Neurocytology. 2002;30:379–390.

40. Yazici B, Gelişken Ö, Avci R, Yücel A. Prediction of visual outcome after retinal detachment surgery using the Lotmar visometer. The British Journal of Ophthalmology. 2002;86(3):278.

41. LaVail MM. Circadian nature of rod outer segment disc shedding in the rat. Investigative ophthalmology & visual science. 1980;19(4):407–411.

42. Kinney MS, Fisher S. Changes in length and disk shedding rate of Xenopus rod outer segments associated with metamorphosis. Proceedings of the Royal Society of London Series B Biological Sciences. 1978;201(1143):169–177.

43. Young RW. The renewal of rod and cone outer segments in the rhesus monkey. The Journal of cell biology. 1971;49(2):303–318.

44. Young RW. Visual cells and the concept of renewal. Investigative ophthalmology & visual science. 1976;15(9):700–725.

45. Baba K, Pozdeyev N, Mazzoni F, Contreras-Alcantara S, Liu C, Kasamatsu M, et al. Melatonin modulates visual function and cell viability in the mouse retina via the MT1 melatonin receptor. Proceedings of the National Academy of Sciences. 2009;106(35):15043–15048.

46. Laurent V, Sengupta A, Sánchez-Bretaño A, Hicks D, Tosini G. Melatonin signaling affects the timing in the daily rhythm of phagocytic activity by the retinal pigment epithelium. Experimental eye research. 2017;165:90–95.

47. Nikolaeva DA, Astakhova LA, Firsov ML. The effects of dopamine and dopamine receptor agonists on the phototransduction cascade of frog rods. Molecular vision. 2019;25:400.

48. Murakami Y, Notomi S, Hisatomi T, Nakazawa T, Ishibashi T, Miller JW, et al. Photoreceptor cell death and rescue in retinal detachment and degenerations. Progress in retinal and eye research. 2013;37:114–140.

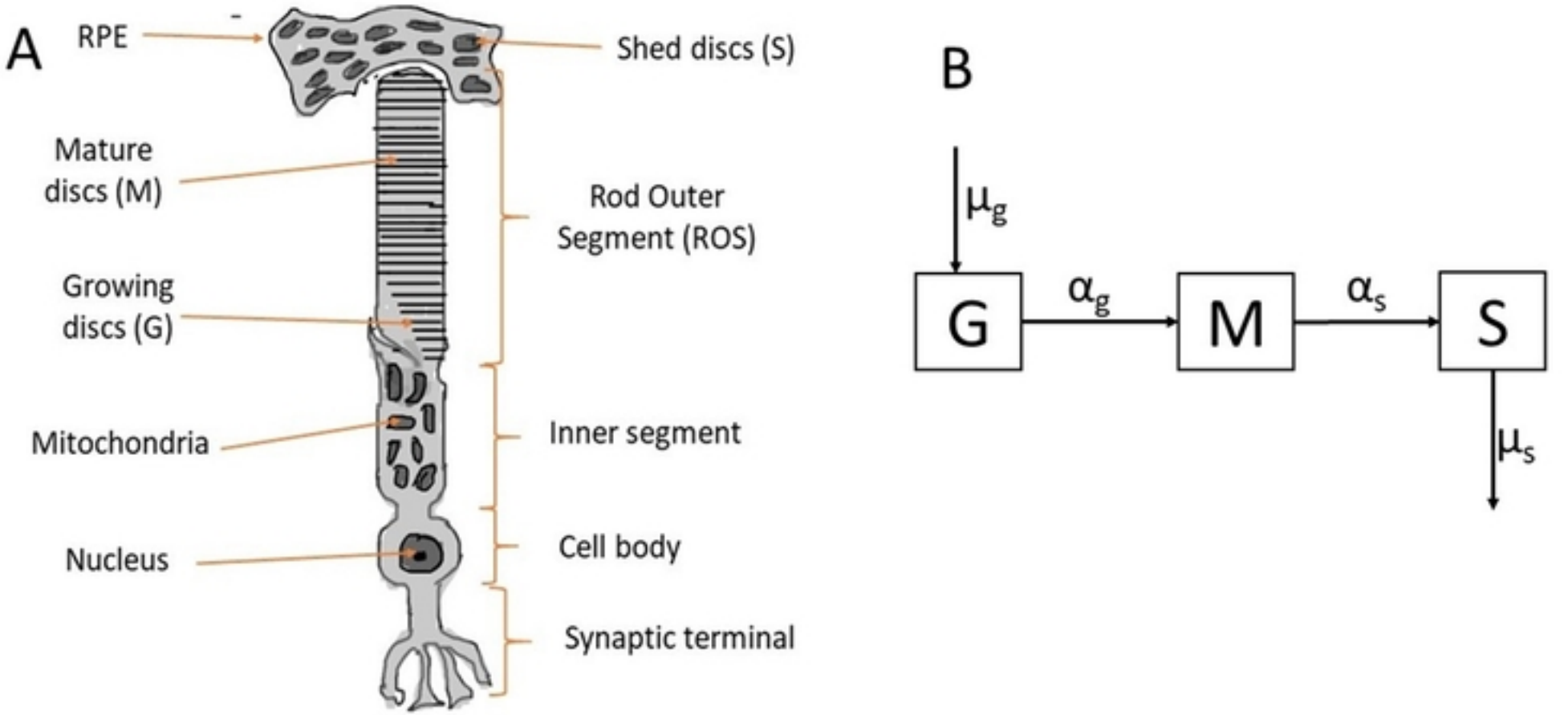
A
RPE
Shed discs (S)
Mature discs (M)
Rod Outer Segment (ROS)
Growing discs (G)
Mitochondria
Inner segment
Nucleus
Cell body
Synaptic terminal
B
μ_g
G
α_g
M
α_s
S
μ_s

Figure 1

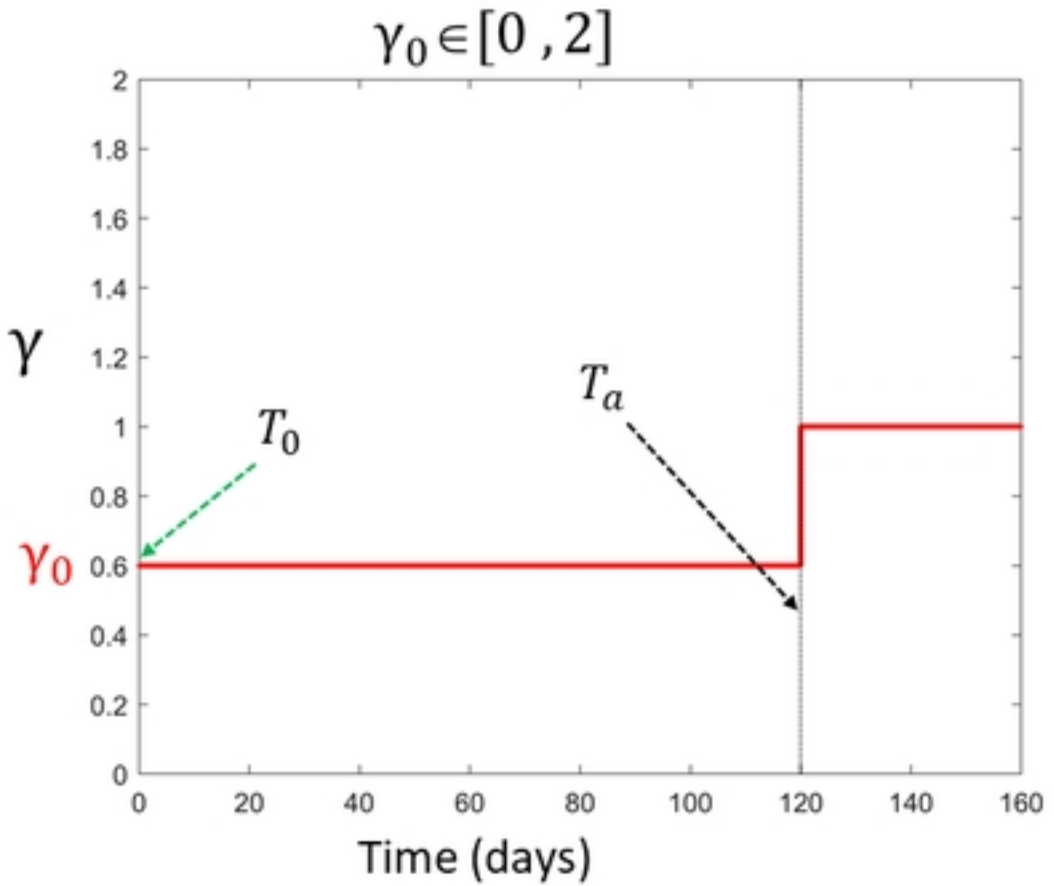
$\gamma_0 \in [0, 2]$
γ
γ_0
T_0
T_a
Time (days)

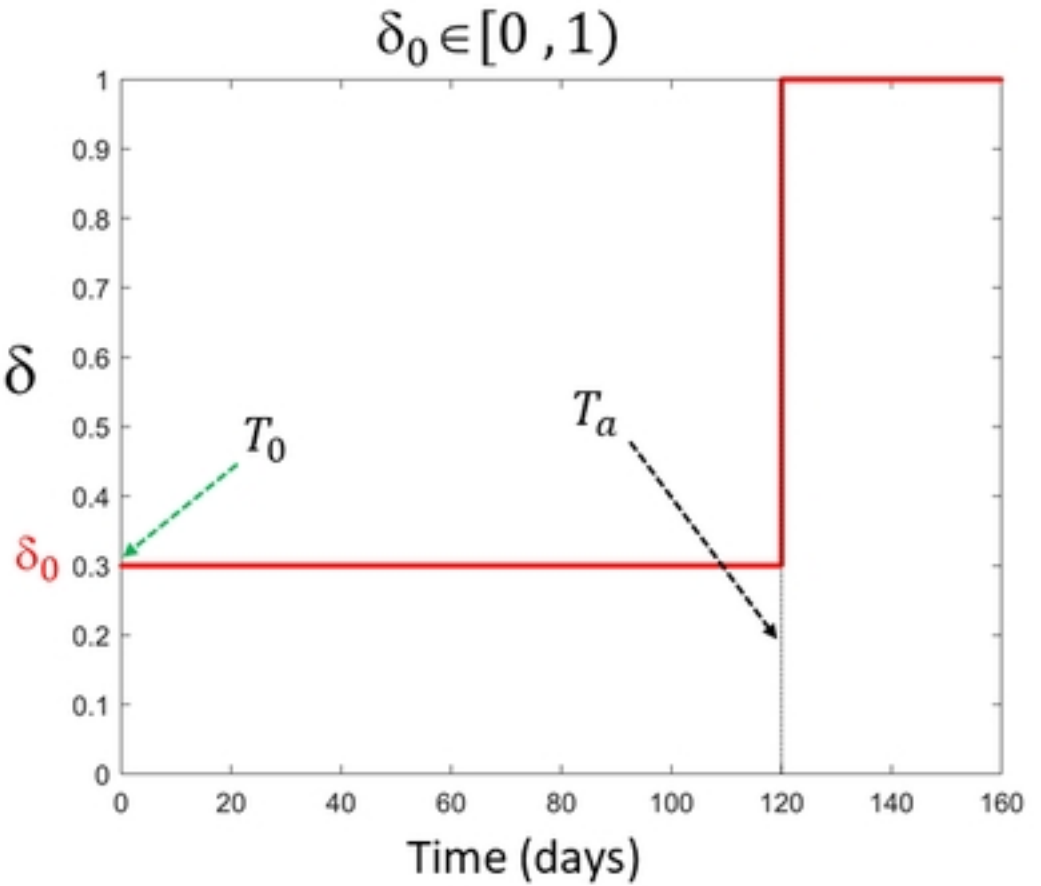
$\delta_0 \in [0, 1)$
δ
δ_0
T_0
T_a
Time (days)

Figure 2

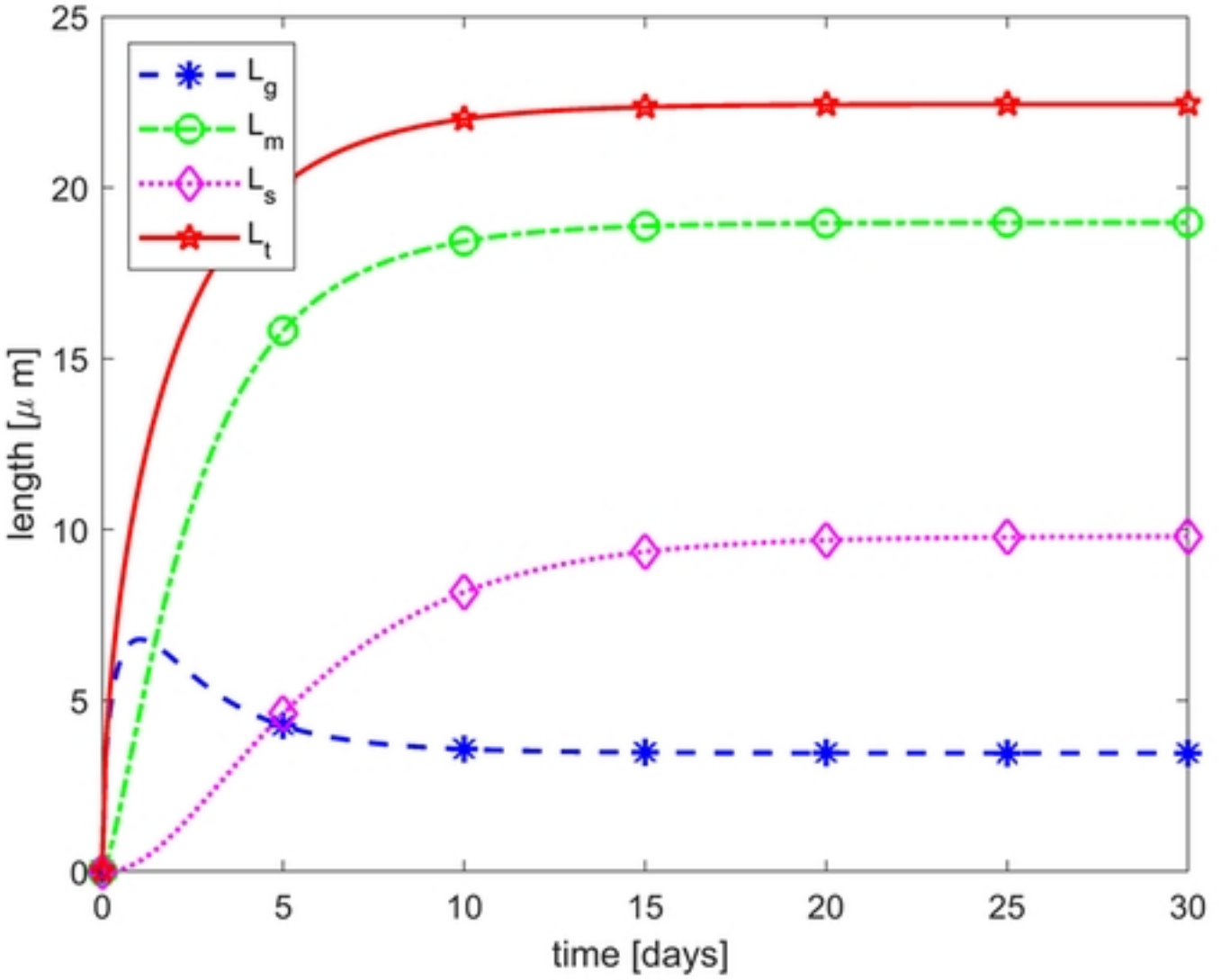

Figure 3

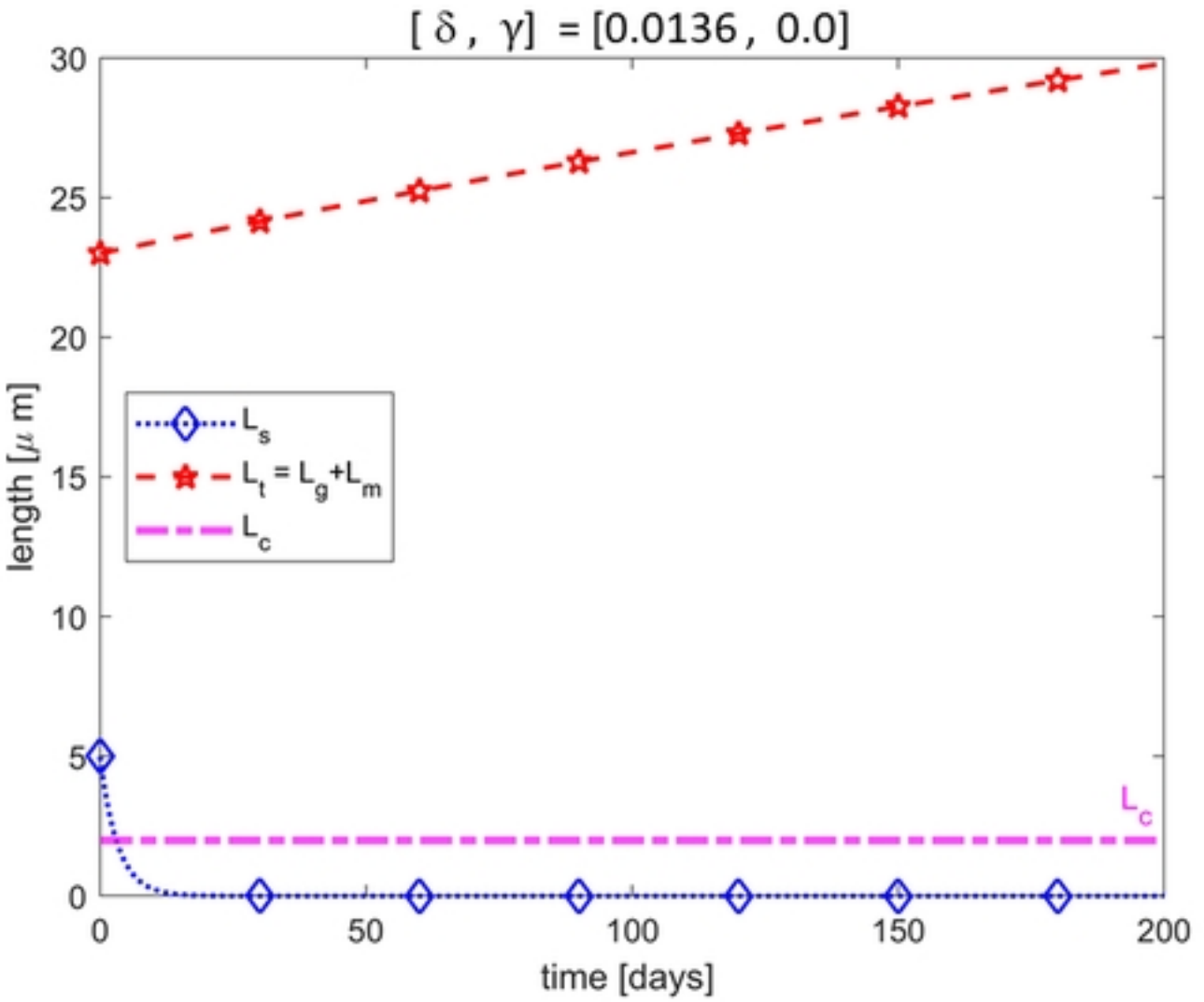
[δ , γ] = [0.0136 , 0.0]
30
25
20
15
10
5
0
length [μ m]
L_s
L_t = L_g+L_m
L_c
L_c
0
50
100
150
200
time [days]

Figure 4

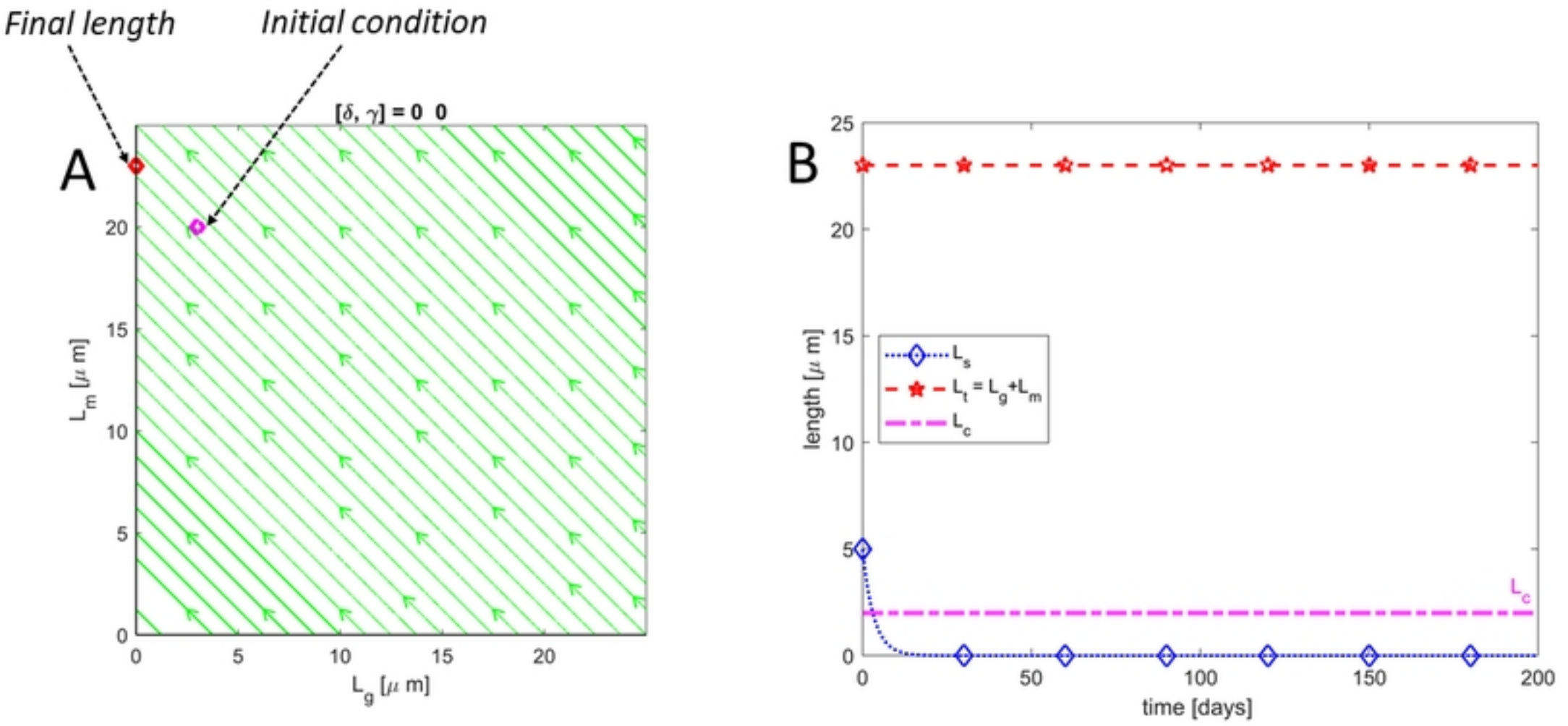
Final length
Initial condition
[δ, γ] = 0 0
A
B
L_m [μ m]
L_g [μ m]
length [μ m]
time [days]
L_s
L_t = L_g+L_m
L_c
0
5
10
15
20
25
50
100
150
200

Figure 5

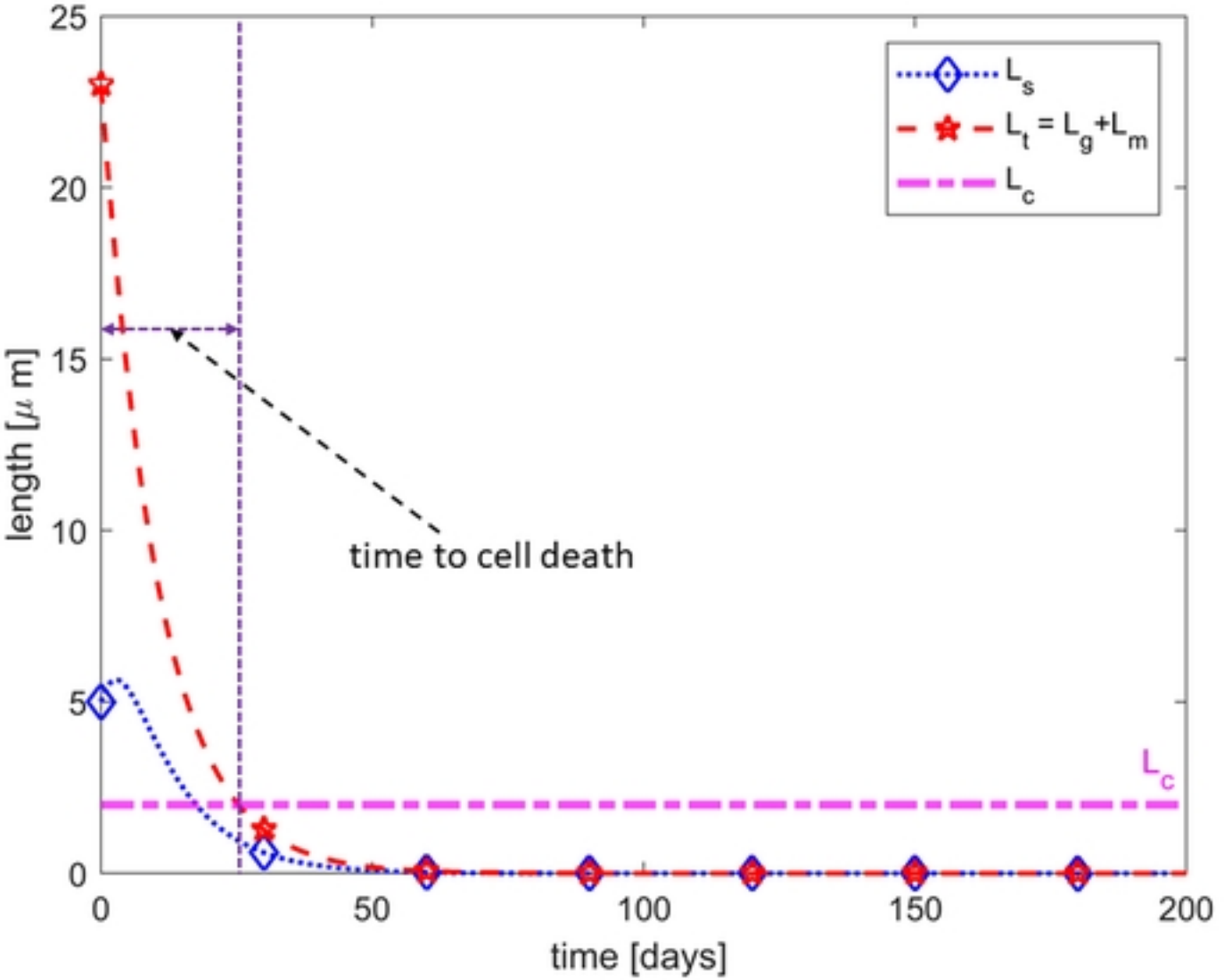
25
20
15
10
5
0
0
50
100
150
200
length [μ m]
time [days]
L_s
$L_t = L_g + L_m$
L_c
time to cell death
L_c

Figure 6

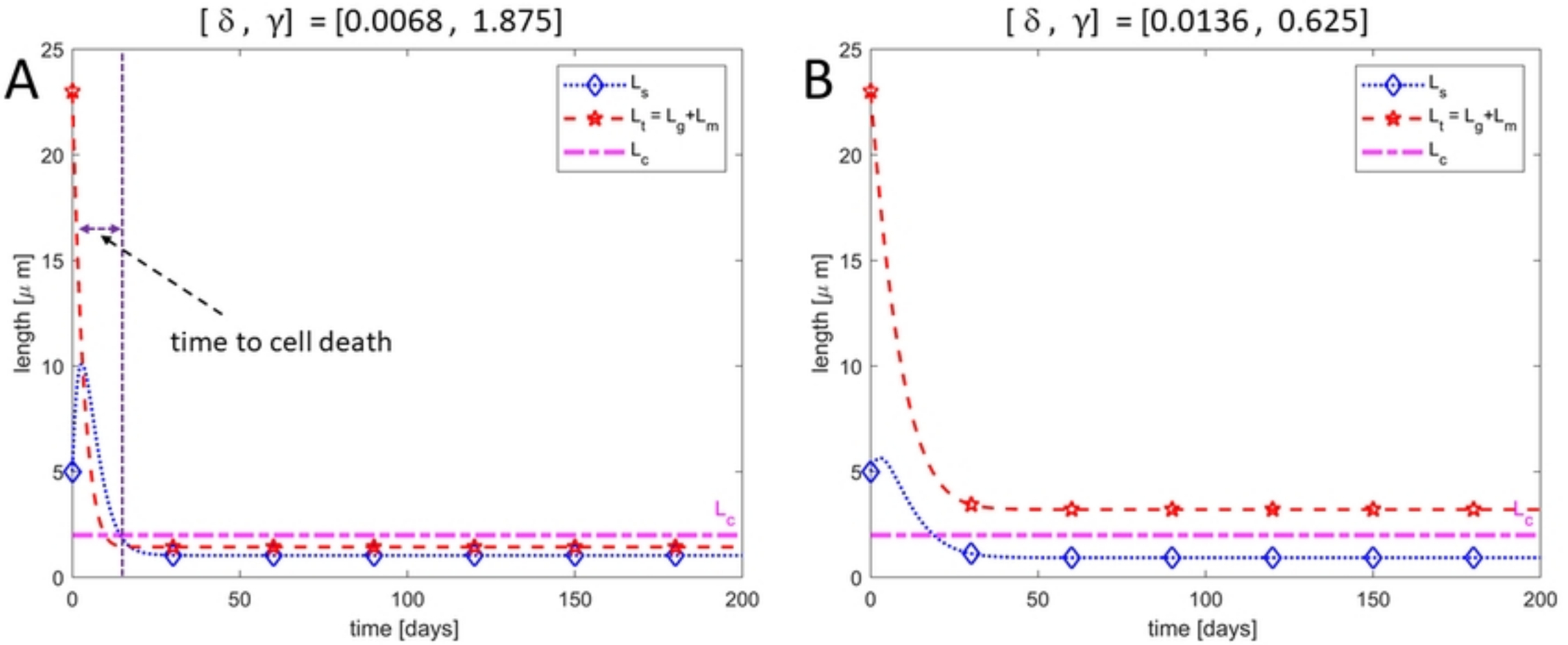
[δ , γ] = [0.0068 , 1.875]
A
25
20
15
10
5
0
length [μ m]
0
50
100
150
200
time [days]
L_s
$L_t = L_g + L_m$
L_c
time to cell death
L_c
[δ , γ] = [0.0136 , 0.625]
B
25
20
15
10
5
0
length [μ m]
0
50
100
150
200
time [days]
L_s
$L_t = L_g + L_m$
L_c
L_c

Figure 7

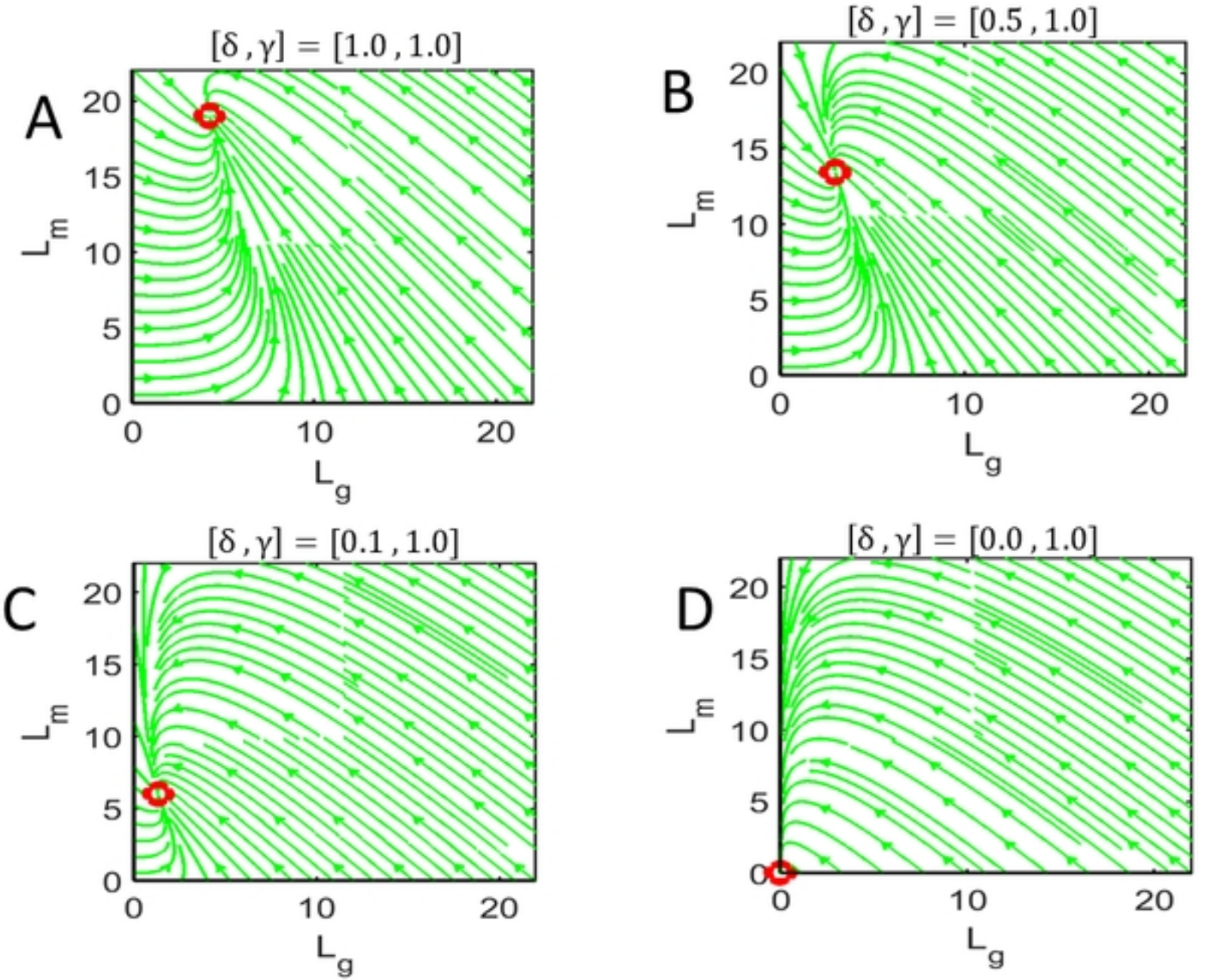

Figure 8

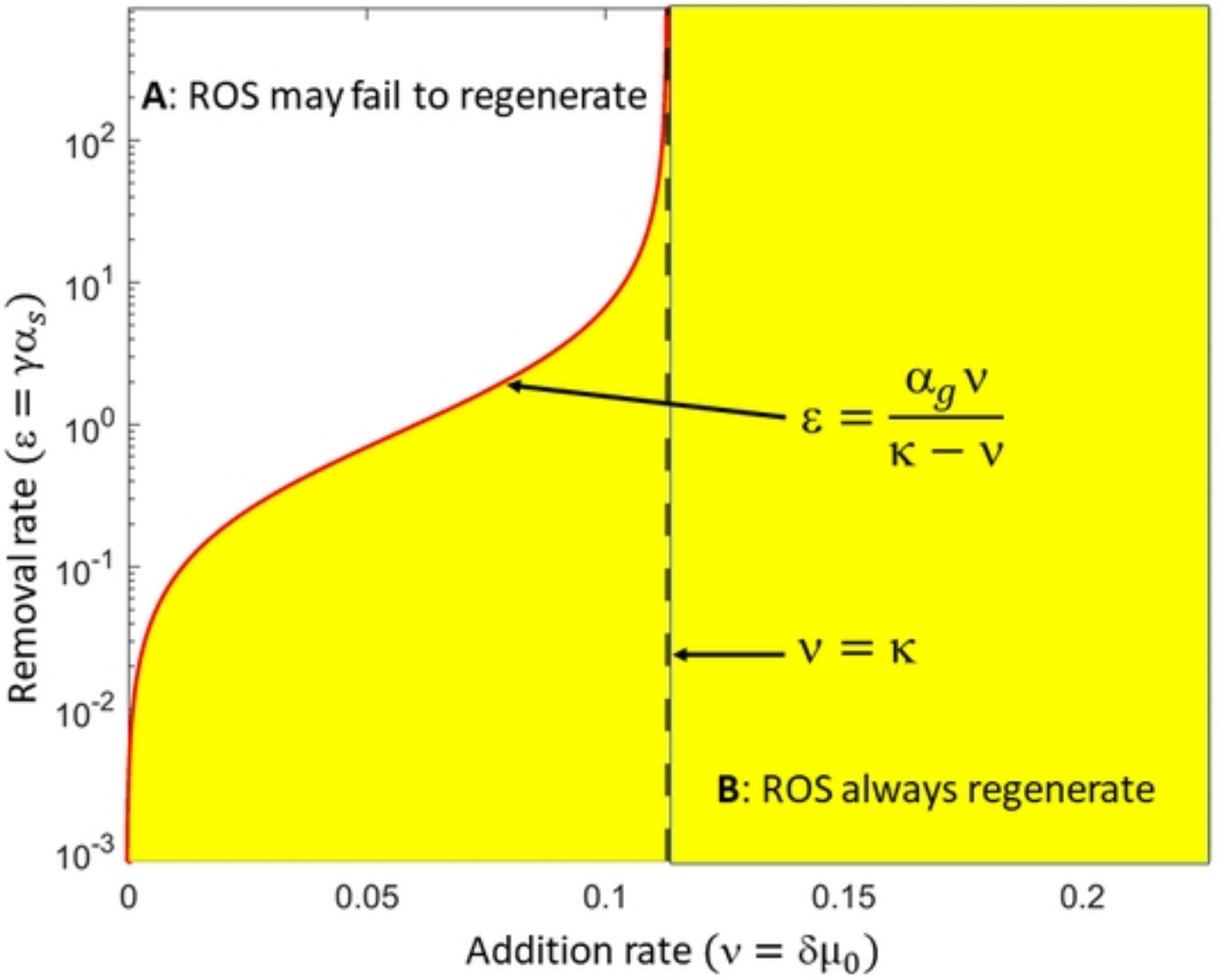
A: ROS may fail to regenerate
B: ROS always regenerate
$\varepsilon = \frac{\alpha_g \nu}{\kappa - \nu}$
$\nu = \kappa$
Removal rate ($\varepsilon = \gamma\alpha_s$)
Addition rate ($\nu = \delta\mu_0$)
10^{2}
10^{1}
10^{0}
10^{-1}
10^{-2}
10^{-3}
0
0.05
0.1
0.15
0.2

Figure 9

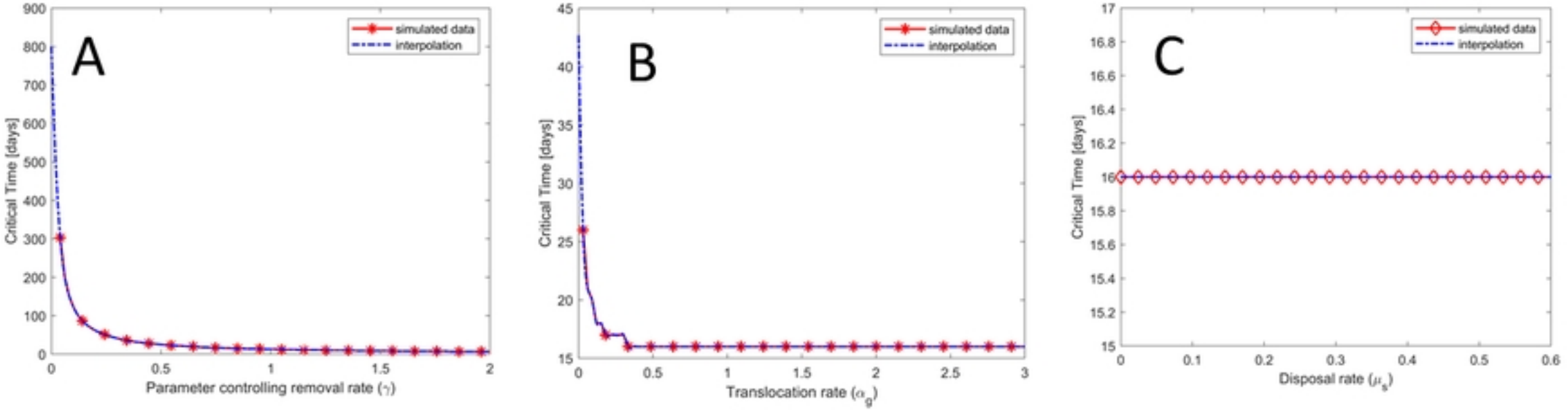
A
simulated data
interpolation
Critical Time [days]
Parameter controlling removal rate (γ)
B
simulated data
interpolation
Critical Time [days]
Translocation rate (α_g)
C
simulated data
interpolation
Critical Time [days]
Disposal rate (μ_s)

Figure 10

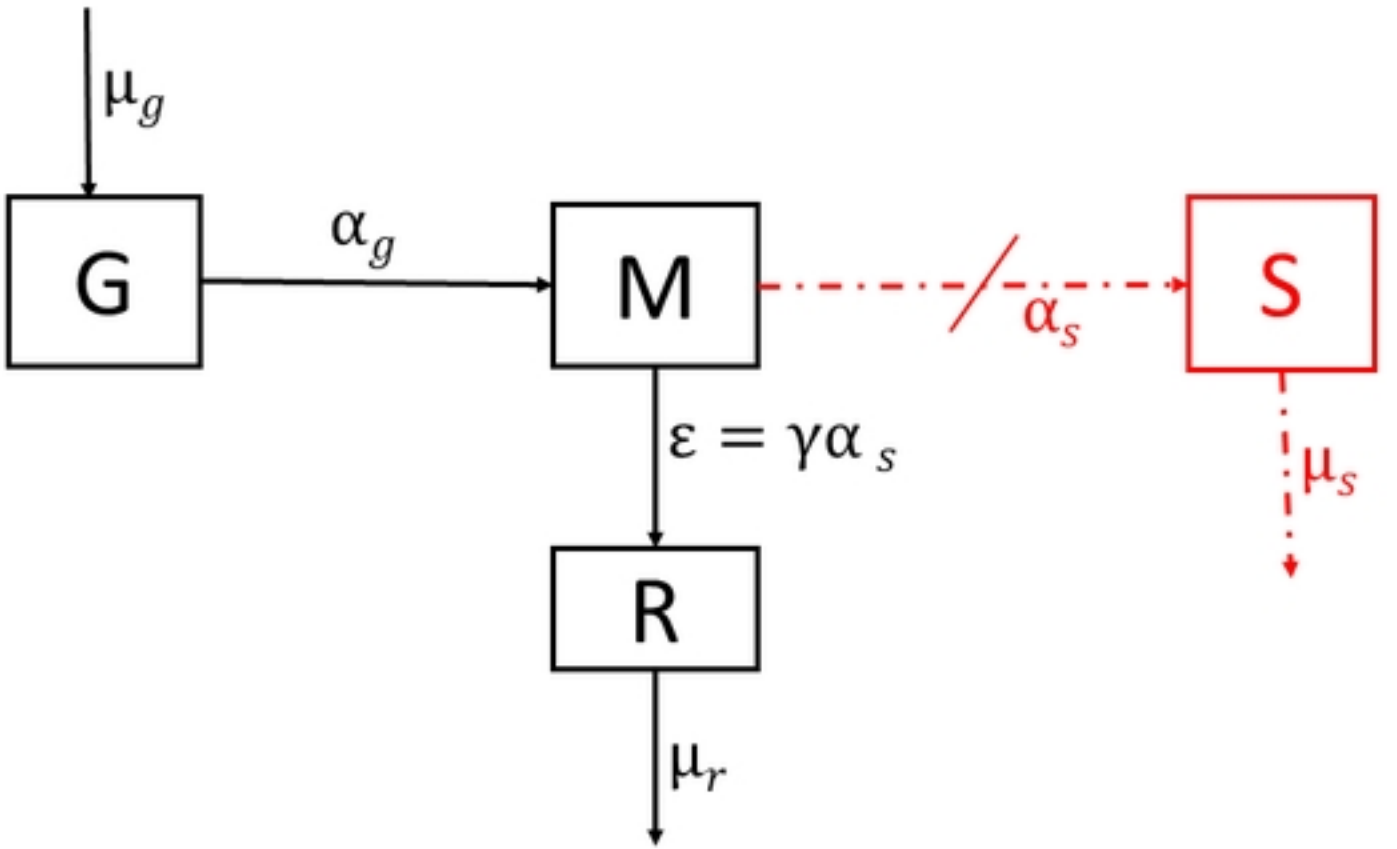

Figure 11